JOURNAL OF SOLID STATE CHEMISTRY

Volume 179, Number 10, October 2006

CONTENTS

Regular Articles

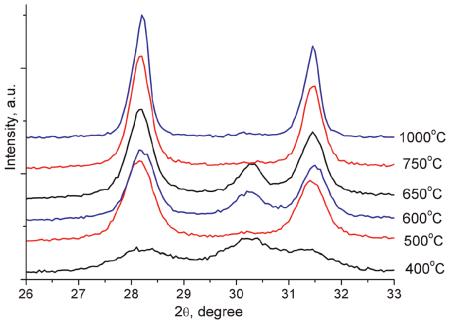

Appearance of the (111) peak of cubic phase at $2\theta \sim 30.5^\circ$ in the diffraction patterns of zirconia samples calcined at 600 and 650 °C could be explained by polysynthetic twinning in zirconia crystallites along the (001) direction.

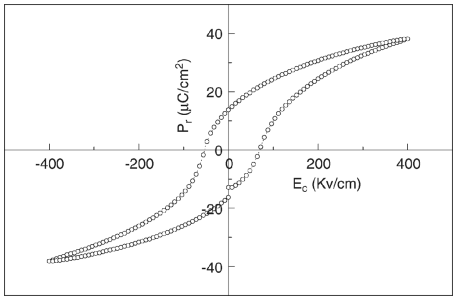

P-E hysteresis loops for BST:Sn film annealed at 700°C for 2 hours in oxygen atmosphere.

Regular Articles—Continued

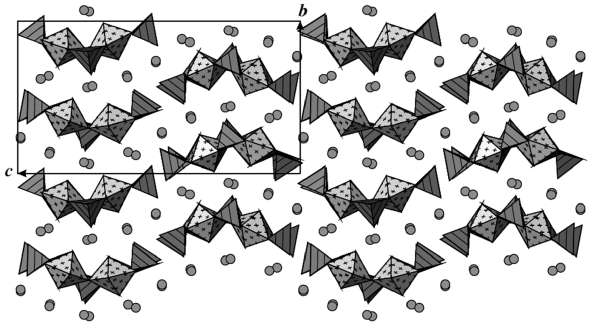

One-dimensional chains in the structure of $Cs_8[(UO_2)_4(WO_4)_4(WO_5)_2]$.

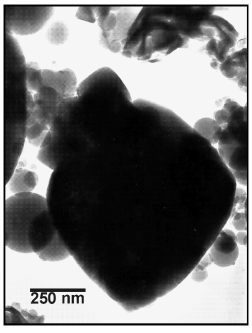

Katoite, $Ca_3Al_2(SiO_4)_{3-x}(OH)_{4x}$ ($0 \leqslant 3-x \leqslant 0.334$), was identified besides gibbsite, $Al(OH)_3$, as a crystalline stable hydration product in $Ca_3Al_2O_6$, $Ca_{12}Al_{14}O_{33}$ and $CaAl_2O_4$ hydrated with added amorphous silica between 40 and 90 °C.

Continued

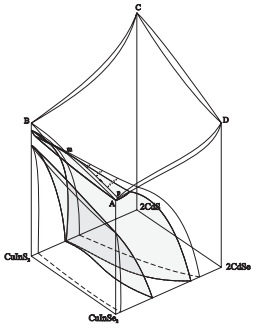

Perspective view of the reciprocal system $CuInSe_2 + 2CdS \Leftrightarrow CuInS_2 + 2CdSe$.

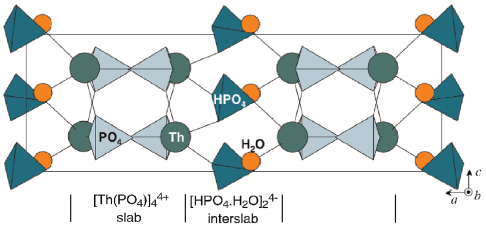

The 2D structure of the TPHPH precursor that sustains first the HPO_4 condensation and dehydration in the interslabs then a shearing of the slabs leading to stable β-TPD, a 3D framework suitable for long-term storage of actinide elements.

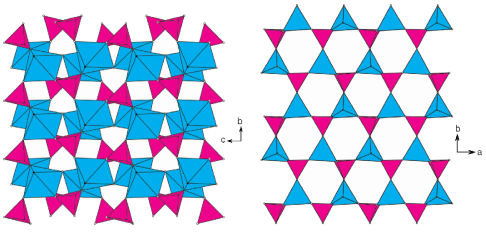

A layered manganese compound $Mn_2(2\text{-}C_5H_4NPO_3)_2(H_2O)$ (**1**) in which chains of aqua-bridged $\{Mn_2O_2\}$ dimers are connected by $\{CPO_3\}$ tetrahedra through corner-sharing and a zinc compound $Zn(6\text{-}Me\text{-}2\text{-}C_5H_4NPO_3)$ (**2**) with a honeycomb layer structure are reported in this paper. Weak antiferromagnetic interactions are propagated between the Mn(II) centers in **1**.

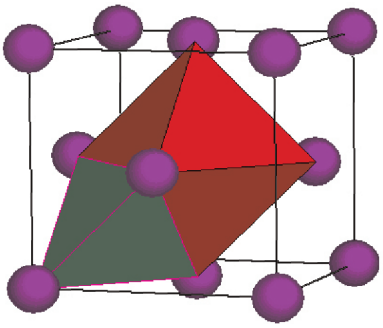

3D view of the crystal structure of $Mg_{0.65}Sc_{0.35}D_{2.2}$.

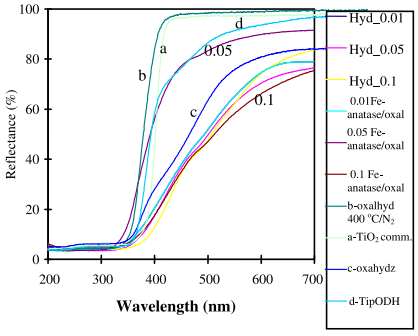

DRS of TiO_2, N/Fe–N doped TiO_2.

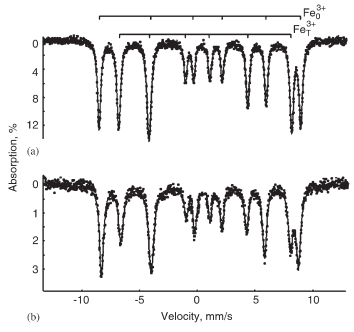

The ^{57}Fe Mössbauer spectra for $Sr_2(Fe_{1-x}Ga_x)_2O_5$ at 80 K: I = 0 (a) and $x = 0.2$ (b).

Magnetic susceptibility, specific heat and magnetic structure of $CuNi_2(PO_4)_2$
Jaione Escobal, José L. Pizarro, José L. Mesa, Aitor Larrañaga, Jesús Rodríguez Fernández, María I. Arriortua and Teófilo Rojo
Page 3052

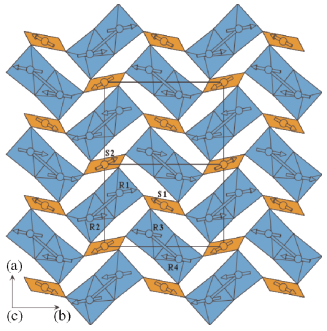

Magnetic structure of $CuNi_2(PO_4)_2$.

Synthesis and structural characterization of two polymorphs of Fe(2,2′-bpy)(HPO_4)(H_2PO_4)
Wen-Jung Chang, Yau-Chen Jiang, Sue-Lein Wang and Kwang-Hwa Lii
Page 3059

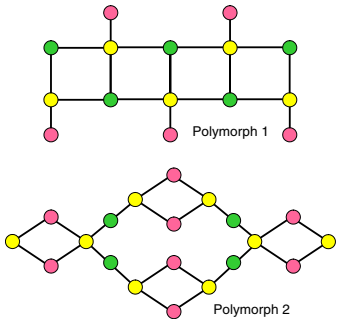

Schematic representation of a section of a chain in polymorph **1** and a layer in polymorph **2**.

Structural investigations of lead–strontium fluoroapatites
Béchir Badraoui, Abdallah Aissa, Adriana Bigi, Mongi Debbabi and Massimo Gazzano
Page 3065

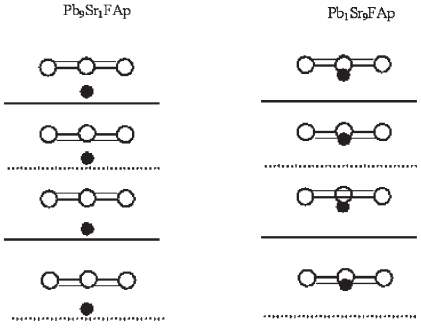

The structural refinements carried out on five $Pb_{(10-x)}Sr_x(PO_4)_6F_2$ samples evidence preferential distribution of cations in metal sites and a progressive shift of the F^- ion.

Rare earth–copper–magnesium compounds $RECu_9Mg_2$ (RE = Y, La–Nd, Sm–Ho, Yb) with ordered $CeNi_3$-type structure
P. Solokha, V. Pavlyuk, A. Saccone, S. De Negri, W. Prochwicz, B. Marciniak and E. Różycka-Sokołowska
Page 3073

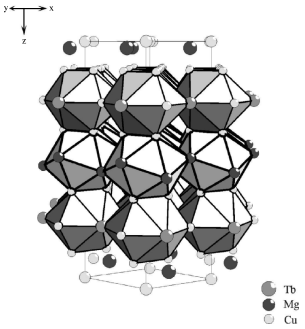

The perspective view of the arrangement of the icosahedrons and anti-cubooctahedrons in the structure of $TbCu_9Mg_2$.

$[C_6H_{21}N_4][Sb_9S_{14}O]$: Solvothermal synthesis, crystal structure and characterization of the first non-centrosymmetric open Sb–S–O framework containing the new $[SbS_2O]$ building unit
Ragnar Kiebach, Christian Näther, C. Peter Sebastian, Bernd D. Mosel, Rainer Pöttgen and Wolfgang Bensch
Page 3082

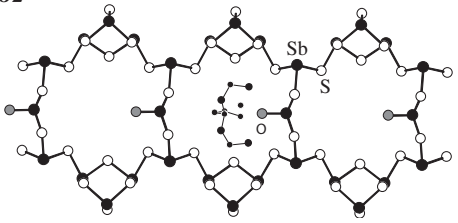

The $[Sb_9S_{14}O]^{3-}$ chain in $[C_6H_{21}N_4][Sb_9S_{14}O]$ directed along the *b*-axis with the organic template molecule acting like a tetradentate ligand around the O atom of the $[SbS_2O]$ group.

Polycationic disorder in $[Bi_6O_4(OH)_4](NO_3)_6$: Structure determination using synchrotron radiation and microcrystal X-ray diffraction
N. Henry, O. Mentré, F. Abraham, E.J. MacLean and P. Roussel
Page 3087

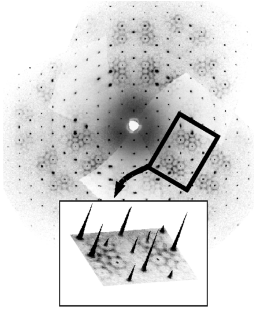

Reconstructed *hk0* precession layer showing intense Bragg peaks and large amount of diffuse scattering.

Continued

Two novel 3-D bismuth oxalates with organic amines protruding in channels

Xiaohong Yu, Hanhui Zhang, Yanning Cao, Zhongjian Hu, Yiping Chen and Zhen Wang

Page 3095

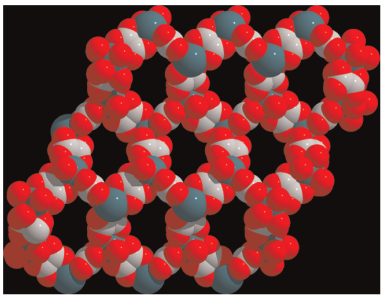

In this work, two novel 3-D oxalate-containing bismuth compounds with channels were obtained by hydrothermal method. In compound **1**, the connectivity between Bi and three oxalates gives rise to a honeycomb-like layer, with a 12-membered aperture in the *ac* plane. Then the layers are also connected through oxalate ligands, creating the 3-D structure with a channel about 5.0 Å × 5.0 Å along the *c*-axis. The uncoordinated water molecules and protonated imidazole molecules were located in the channels.

Crystal structures of lanthanide and zirconium phosphates with general formula $Ln_{0.33}Zr_2(PO_4)_3$, where Ln = Ce, Eu, Yb

D.M. Bykov, E.R. Gobechiya, YuK Kabalov, A.I. Orlova and S.V. Tomilin

Page 3101

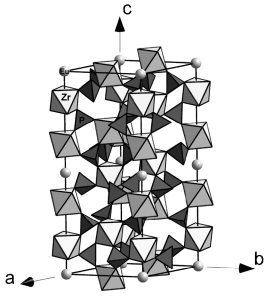

Fragment of structure of synthetic phosphate $Eu_{0.33}Zr_2(PO_4)_3$.

The crystal structure, thermal behaviour and ionic conductivity of a novel lithium gadolinium polyphosphate $LiGd(PO_3)_4$

Hasna Ettis, Houcine Naïli and Tahar Mhiri

Page 3107

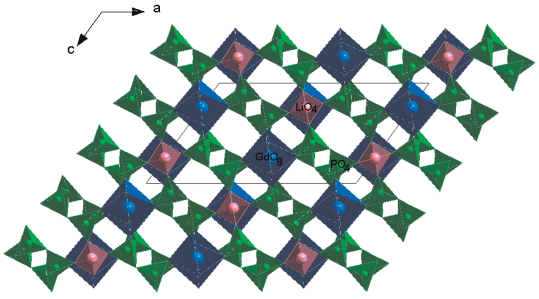

The structural arrangement of $LiGd(PO_3)_4$ viewed in the (0 1 0) plane.

Preparation of 5-benzotriazolyl-4-hydroxy-3-*sec*-butylbenzenesulfonate anion-intercalated layered double hydroxide and its photostabilizing effect on polypropylene

Dianqing Li, Zhenjun Tuo, David G. Evans and Xue Duan

Page 3114

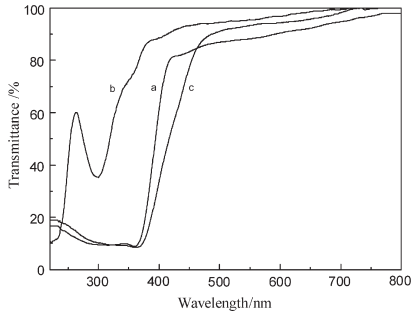

Intercalation of an organic UV absorber in a layered double hydroxide host leads to an enhancement of its photo- and thermal stability.

Effect of Cr-doping on charge ordering stability in $Bi_{1-x}Sr_xMn_{1-y}Cr_yO_3$

Shigeki Yamada, Eri Sugano and Taka-hisa Arima

Page 3121

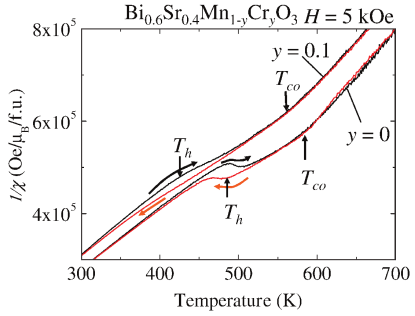

Temperature dependence of $Bi_{0.6}Sr_{0.4}Mn_{1-y}Cr_yO_3$ (y = 0, 0.1). The abbreviation 'f.u.' denotes the formula unit. T_{co} and T_h are represented kinks or anomalies that involve hysteresis, respectively.

Stuffed rare earth pyrochlore solid solutions

G.C. Lau, B.D. Muegge, T.M. McQueen, E.L. Duncan and R.J. Cava

Page 3126

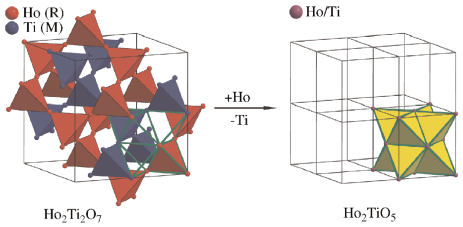

A simplified model of the transition from pyrochlore to fluorite in the series $Ln_2(Ti_{2-x}Ln_x)O_{7-x/2}$ (Ln = Tb–Lu, $0 \leqslant x \leqslant 0.67$), with Ho as an example. The separate corner sharing tetrahedral lattices of cations in the pyrochlore structure develop into edge sharing tetrahedra as extra Ln is stuffed in place of Ti. The increased spin connectivity in these new materials represents a new avenue of study in the well-known rare earth titanate pyrochlores in view of geometrical magnetic frustration.

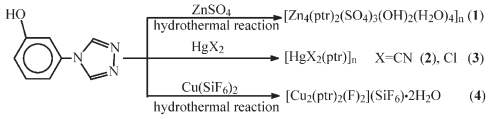

Four triazole-bridging coordination complexes, $[Zn_4(ptr)_2(SO_4)_3(\mu_3\text{-}OH)_2(H_2O)_4]_n$ (**1**), $[Hg(CN)_2(ptr)]_n$ (**2**), $[Hg(Cl)_2(ptr)]_n$ (**3**) and $[Cu_2(\mu_2\text{-}ptr)_2(\mu_2\text{-}F)_2]_n(SiF_6)_n \cdot 2nH_2O$ (**4**), were synthesized with (*m*-phenol)-1,2,4-triazole (ptr). Compounds **1–4** with extended structures of 4-substituted 1,2,4-triazole are rarely reported.

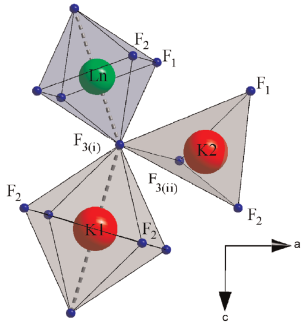

The coordination polyhedra of *Ln*, K(1) and K(2) atoms along *b* direction in K_3LnF_6.

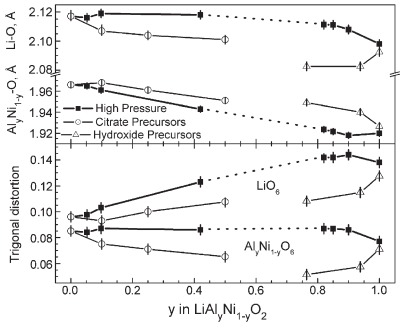

The incorporation of Al into the layered structure of $LiNiO_2$ is limited.

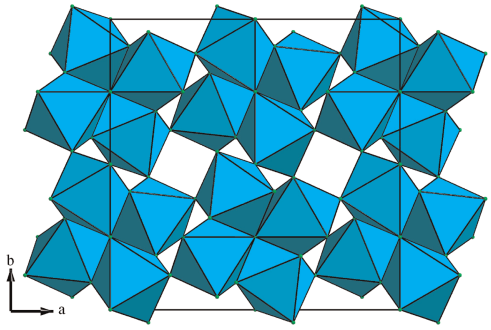

Hypothetical AlF_3 structure with a dense packing of corner-sharing AlF_6 octahedra packed in tetrahedral blocks.

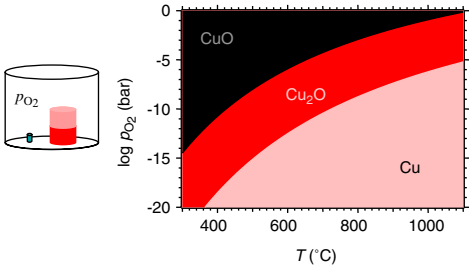

Oxygen nonstoichiometry control by p_{O_2} buffer.

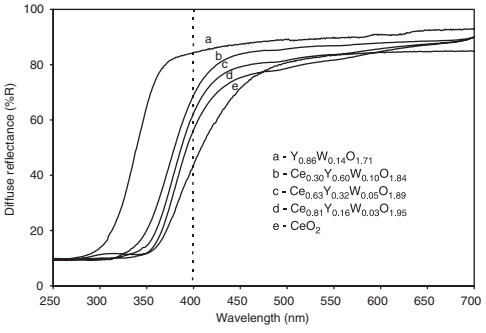

Diffuse reflectance spectra of the Ce-Y-W-O samples calcined at 1000 °C.

Continued

Synthesis and crystal structure of a novel ternary oxoborate, $PbBiBO_4$

Xuean Chen, Jianlong Zuo, Xinan Chang, Yinghua Zhao, Hegui Zang and Weiqiang Xiao

Page 3191

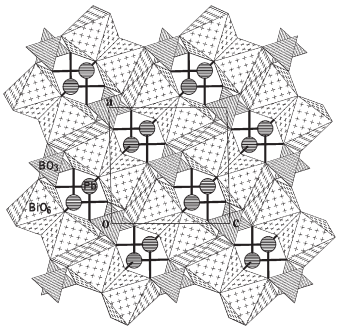

$PbBiBO_4$ represents a new structure type in which $^{2}_{\infty}[BiO_4]^{5-}$ layers are bridged by B atoms of BO_3 triangles to give rise to a three-dimensional framework. Channels parallel to the [0 1 0] direction accommodate Pb^{2+} cations.

Synthesis and characterization of hollandite-type material intended for the specific containment of radioactive cesium

A.Y. Leinekugel-le-Cocq, P. Deniard, S. Jobic, R. Cerny, F. Bart and H. Emerich

Page 3196

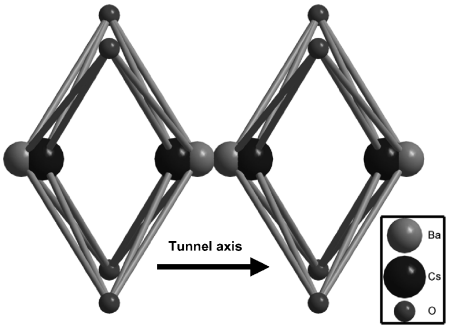

Ba and Cs location along the tunnel axis in $BaCs_{0.28}Fe_{0.82}Al_{1.46}Ti_{5.72}O_{16}$.

A new three-dimensional cobalt phosphate: $Co_5(OH_2)_4(HPO_4)_2(PO_4)_2$

Zhangang Han, Aixiang Tian, Jun Peng and Xueliang Zhai

Page 3209

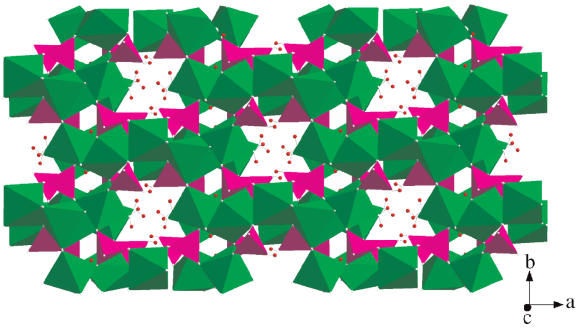

A 3D cobalt phosphate with a neutral framework, $Co_5(OH_2)_4(HPO_4)_2(PO_4)_2$ (**1**), has been synthesized and characterized. Compound **1** exhibits a complex net architecture based on edge- and corner-sharing of CoO_6 and PO_4 polyhedra. Its magnetic property was researched.

Solid-state structural properties of 2,4,6-trimethoxybenzene derivatives, determined directly from powder X-ray diffraction data in conjunction with other techniques

Zhigang Pan, Mingcan Xu, Eugene Y. Cheung, James A. Platts, Kenneth D.M. Harris, Edwin C. Constable and Catherine E. Housecroft

Page 3214

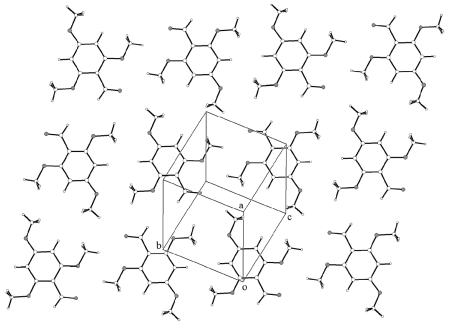

Final Rietveld refinement for 2,4,6-trimethoxyacetophenone.

Magnetic properties of RY_2Ni_9 compounds and their hydrides (R = La, Ce)

V. Paul-Boncour, M. Latroche and A. Percheron-Guégan

Page 3224

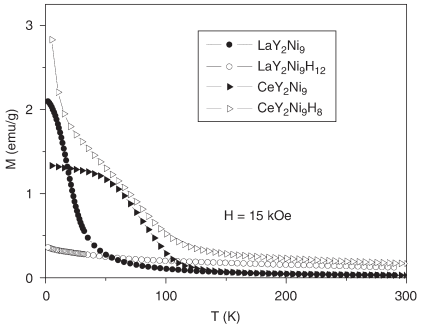

This figure shows the isofield magnetization measured at 15 KOe of the RY_2Ni_9 compounds and their hydrides (R = La, Ce).

Solvothermal synthesis and characterisation of $La_{1-x}A_xMnO_3$ nanoparticles

Carlos Vázquez-Vázquez and M. Arturo López-Quintela

Page 3229

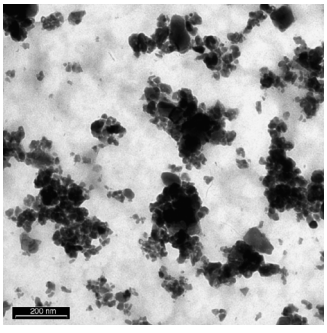

TEM of $LaMnO_3 + \delta$ calcined at 600 °C.

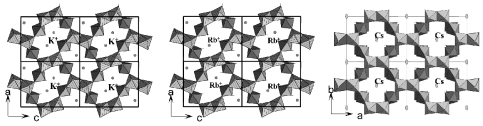

Occupation of the tunnels of the uranium niobium polyhedra framework by the alkaline metal in (a) $KUNbO_6$, (b) $Rb_{0.5}UNbO_{5.75}$ and (c) $Cs_{0.5}UNbO_{5.75}$.

Rapid Communications

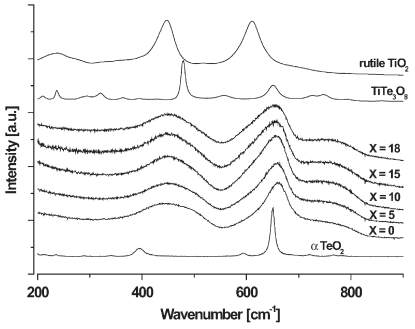

Raman spectra of the titanium tellurite glasses and of the relevant crystalline compounds.

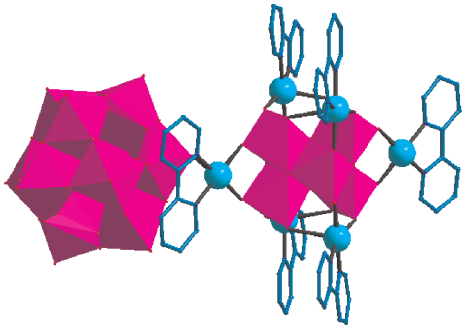

A novel polyoxometalate $[\{Cu(2,2'\text{-bpy})\}_6(Mo_6O_{22})][GeMo_{12}O_{40}] \cdot H_2O$, which represents the first example of 1D organic–inorganic hybrid based on a Keggin-type heteropolyanion $[GeMo_{12}O_{40}]^{4-}$ and an unprecedented isopolyanion $[Mo_6O_{22}]^{8-}$.

NOTICE

The Keyword Index for Volume 179 will appear in the December 2006 issue as part of a cumulative index for the year 2006.